ARTICLE

Circular RNA CLASP1 modulates the GLI1/SNAIL axis and enhances macrophage polarization in breast cancer

Lijun Zhou[1,7], Mei Liu[2,7], Fujun Liu[3], Zhengkun Wang[1], Xinyu Li[4], Xiaoyu Peng[1], Wenqiang Ma[1], Peilan Guo[1], Lifang Yuan[3], Slawomir Wolczynski[5], Nafis Ahmed Rahman[5,6], Wei Song[4] and Xiangdong Li[1,5]✉

Breast cancer (BC) is the most prevalent malignancy among women worldwide. Growing evidence highlights the crucial role of circular RNAs (circRNAs) in BC carcinogenesis; however, their underlying mechanisms remain largely unknown. In this study, we identify circCLASP1, which is significantly upregulated in BC tissues ($n = 65$) and serum samples ($n = 61$). Its expression correlates with lymph node metastasis, ki67 expression, and tumor size. Receiver operation characteristic (ROC) curve analysis reveals area under the curve (AUC) values of 0.8196 (BC tissues) and 0.8902 (BC serum), respectively. Functionally, circCLASP1 knockdown significantly suppresses BC cell proliferation, migration, and invasion. Mechanistically, circCLASP1 prevents the ubiquitin-mediated degradation of GLI1 protein by facilitating its interaction with CCT2, thereby stabilizing GLI1. Moreover, circCLASP1 enhances the nuclear accumulation of GLI1, leading to increased *SNAIL* expression and thereby upregulating the expression of *CCL2* and *CCL5*, which in turn promotes macrophage M2 polarization, ultimately resulting in BC progression and subsequent lung metastasis. Further analysis reveals that U2AF2 regulates circCLASP1 biogenesis. Collectively, these findings demonstrate that circCLASP1 promotes BC progression and an immunosuppressive microenvironment via the CCT2/GLI1/SNAIL axis, highlighting its potential as a prognostic biomarker and therapeutic target for BC.

Oncogene (2025) 44:4765–4780; https://doi.org/10.1038/s41388-025-03627-2

Graphical Abstract

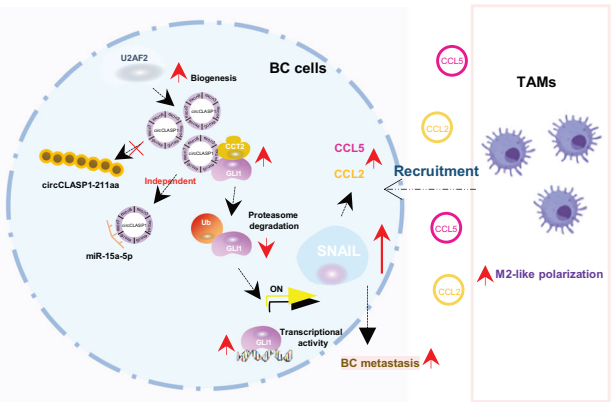

INTRODUCTION

Breast cancer (BC) is the most common cancer worldwide, accounting for ~11.6% of new cancer cases, with a mortality rate of 6.9% [1]. BC is pathologically classified into four clinical subtypes: Luminal A, Luminal B, human epidermal growth factor receptor 2-positive (HER2+), and triple-negative breast cancer (TNBC) [2]. The progression of BC is driven by multiple risk factors, including hormonal disorders, genetic predispositions, environmental influences, diets, and others [3, 4]. Despite advancements in the early-stage diagnosis and treatment of BC, many patients

[1]State Key Laboratory of Animal Biotech Breeding, College of Biological Sciences, China Agricultural University, Beijing, China. [2]Department of Pathology, The Sixth Medical Center of Chinese PLA General Hospital, Beijing, China. [3]Shandong Stem Cell Engineering Technology Research Center, Yantai Yuhuangding Hospital Affiliated to Qingdao University, Shandong, China. [4]Shandong Provincial Hospital Affiliated to Shandong First Medical University, Shandong, China. [5]Department of Reproduction and Gynecological Endocrinology, Medical University of Bialystok, Bialystok, Poland. [6]Department of Physiology, Institute of Biomedicine, University of Turku, Turku, Finland. [7]These authors contributed equally: Lijun Zhou, Mei Liu. ✉email: xiangdongli68@126.com

Received: 6 May 2025 Revised: 23 October 2025 Accepted: 4 November 2025
Published online: 17 November 2025

still experience disease progression to advanced stages, even with effective treatments, for reasons that remain unclear [5]. Therefore, identifying new molecular mechanisms underlying BC progression is crucial.

Circular RNAs (circRNAs) are a class of back-spliced single-strand RNAs, synthesized by the back-splicing of pre-mRNAs, and form a covalent-linked closed-loop structure without the 5′ cap or 3′ tail [6]. CircRNAs are highly conserved due to their covalent loop structure and exhibit various biological functions, such as acting as sponges for microRNAs (miRNAs), RNA-binding proteins (RBPs), or even functional oligopeptides [7]. CircRNAs have garnered increasing scientific attention, especially in the context of cancer pathogenesis, providing valuable insights into clinical diagnosis, monitoring, and treatment [8, 9]. Recently, we reported that circCAPG promotes TNBC development via translating a novel oligopeptide [10]. However, the understanding of the pathological role of circRNAs in BC progression remains limited, highlighting the need for further mechanistic research.

Tumor-associated macrophages (TAMs), a significant component of the tumor microenvironment (TME), have been shown to play a critical role in BC [11]. It has been reported that TAMs engage in a 'cancer-immune cell' crosstalk [12], although the underlying mechanisms remain unclear. Thus, exploring the key mechanisms of this multicellular crosstalk could offer valuable insights for developing effective therapeutic strategies to improve the prognosis of BC patients.

By re-analyzing the GEO dataset (GSE71651) derived from clinical BC patient samples, we found that circCLASP1 was significantly overexpressed in BC tissues and serum. ROC analysis showed that circCLASP1 exhibited high sensitivity and specificity, with its expression positively correlated with lymph node metastasis, ki67 expression, histologic grade and tumor size. Therefore, we aimed to clarify the molecular role of circCLASP1, and explore its potential as a biomarker for BC.

MATERIALS AND METHODS

Patients and clinical samples

In this study, BC tissues were collected from patients treated in the Shandong Provincial Hospital Affiliated to Shandong First Medical University, including BC tissues ($n = 65$), para-cancer tissues ($n = 42$), BC serum ($n = 61$), and normal serum ($n = 10$). None of the above-mentioned patients received the chemotherapy or radiation therapy before the surgery.

The organoid model was derived from the BC patients, the protocol was followed as previously described [10, 13]. This study was authorized by the Ethics Committee of Shandong Provincial Hospital Affiliated to Shandong First Medical University (SWYX-NO. 2022-293).

Bioinformatic analysis

For circRNA differential expression analysis, RNA-seq data from NCBI GEO (GSE71651) were downloaded and processed using the DCC package to generate spliced reads, standardized by DESeq2. CircAnno annotated circRNAs based on Ensembl GTF (v104) and circBase. Differentially expressed mRNAs were obtained from TCGA and analyzed via RTCGA and EdgeR. Fold changes and *P* values were calculated using DESeq2, with candidates selected based on log(fold change)≥2.0 and $P \leq 0.05$.

Cell culture

Human breast cancer cell lines (MCF-7, ZR-75-1, SK-BR-3, MDA-MB-231, MDA-MB-468, and Hs578T), HEK-293T, MCF-10A, and THP-1 were purchased from the National Biomedical Laboratory Cell Resource Bank (Shanghai, China). HEK-293T, MCF-7, Hs578T, and MCF-10A were cultured in DMEM-HG or DMEM/F12 media with supplements. ZR-75-1 and THP-1 used RPMI-1640 (31800, Solarbio, China), SK-BR-3 used McCoy's 5a (M9420, Solarbio, China), and MDA-MB-231/MDA-MB-468 used L-15 (L620KJ, Basal Media, China), all containing 10% FBS and necessary additives. Cells were maintained at 37 °C in 5% CO_2, except MDA-MB-231/MDA-MB-468, which were cultured in normal air.

RNA extraction, reverse transcription PCR (RT-PCR) and quantitative reverse transcription PCR (RT-qPCR)

Total RNA was extracted using Trizol® (Yeasen, China) per the manufacturer's instructions, with paraffin-embedded tissues pre-treated by dewaxing and lysis. After spectrophotometric quantification, cDNA was synthesized using M-MLV reverse transcriptase (Accurate Biotechnology, China). RT-qPCR was performed with 2×RealStar Power SYBR qPCR Mix (Genestar, China), and relative gene expression was calculated using the $2^{-\triangle\triangle Ct}$ method.

Actinomycin D (ACTD) assay

BC cell lines were treated with 1 μg/ml ACTD (Sigma-Aldrich, USA), circCLASP1 and linear *CLASP1* mRNA expression were analyzed by RT-qPCR at specific time points.

RNase R treatment

Total RNA from BC cell lines was split into two fractions: one treated with 3 U/mg RNase R, the other with RNase-free water as a control. After 30 min incubation at 37 °C, circCLASP1 and linear *CLASP1* expression were analyzed by RT-qPCR.

Nucleus and cytoplasm separation

The nuclear and cytoplasmic fractions of RNA were separated and extracted using the Paris kit (Invitrogen, USA) according to the manufacturer's instructions.

Plasmid construction, lentiviral infection, and oligonucleotide synthesis

The pLO5-ciR plasmid (Geneseed, Guangzhou, China) containing circCLASP1 was constructed for circCLASP1 overexpression, while two shRNAs targeting its back-splicing site were cloned into pLKO.1-TRC for knockdown. U2AF2 and PTBP1 coding sequences were inserted into pLV-puro for overexpression. Vectors (sh-scramble, pLV-puro, sh-circCLASP1-1/2, pLO5-ciR, pLO5-ciR-circCLASP1, pLV-O5-ciR-circCLASP1-EGFP(2A)-puro, pLV-U2AF2, pLV-PTBP1, pLV-O5-ciR-EGFP, pLV-O5-circCLASP1-EGFP, sh-SNAIL, pLO5-circCLASP1 2 sites MUT) were co-transfected with psPAX2 and pMD2.G into HEK-293T cells. Lentivirus-containing supernatant was collected at 48–72 h, filtered (0.45 μm, Millipore, USA), and used to infect BC cells, followed by puromycin selection for one week. miR-15a-5p-mimics and NC-mimics (Genepharma, Shanghai, China) were transfected using Hieff Trans® siRNA/miRNA (Yeasen, China). Sequences are in Supplementary Table S2.

Cell proliferation assay

For the cell proliferation assay, treated BC cells were seeded into 96-well plates, and viability was assessed using CCK-8 (Beyotime, China) at 450 nm. For the colony formation assay, treated cells were cultured in six-well plates for 14–30 days. For ki67 immunofluorescence, cells were fixed with formalin, permeabilized with TBST, incubated overnight with anti-ki67 antibody (1:1000, CST, USA) at 4 °C, followed by a fluorescent secondary antibody and DAPI nuclear staining (Solarbio, China).

Cell migration and invasion assay

The transwell (84051ES48, Yeasen, China) was used to detect the migration and invasion capacity of cells. For migration assay, the treated cells were seeded into the inner chamber and incubated for 24 h. For invasion assay, firstly, the inner chamber was pretreated with a thin layer of Matrigel (40183ES10, Yeasen, China) diluted by the serum-free medium. Subsequently, the cells were seeded into the chamber and incubated for 24 h.

Flow cytometry assay

Flow cytometry was performed using the Cell Cycle and Apoptosis Analysis Kit (40301ES60, Yeasen, China) and the Annexin V-FITC/PI Apoptosis Detection Kit (40302ES60, Yeasen, China) according to the manufacturer's instructions.

RNA-protein immunoprecipitation (RIP)

RIP assays were performed using an Immunoprecipitation Kit (Beyotime, China) following the manufacturer's instructions. Cells were lysed in buffer with RNase and protease inhibitors, and magnetic beads pre-incubated

with anti-U2AF2, anti-AGO2, anti-CCT2, and anti-GLI1 at room temperature (15 min–1 h). Lysates were immunoprecipitated overnight at 4 °C, and RNA complexes purified and quantified by RT-qPCR. Normal rabbit/mouse IgG served as the control, with a general unconjugated secondary antibody (Abcam, USA).

Western blot and immunoprecipitation (IP) assay

Total protein was extracted by the ProteinExt® Mammalian Total Protein Extraction Kit (DE101-01, TransGen Biotech, China). After the electrophoresis with SDS-PAGE gel, protein bands were transferred onto the PVDF membrane (Millipore, USA), and subsequently incubated with the primary antibody, and HRP-conjugated secondary antibody. The chemiluminescent signal was visualized on a Western blot imaging system (Vilber, France). Preparation and analysis of Co-IP were described earlier [14]. The following antibodies were used in the study: anti-GAPDH (60004-1-Ig, Proteintech, China), anti-BAX (A12009, ABclonal, China), anti-BCL2 (A-01203, Shanghai hengyuan biological technology co., LTD, China), anti-CDK4 (AtaGenix Laboratories Co., Ltd, Wuhan, China), anti-U2AF2 (A4552, ABclonal, China), anti-DYKDDDDK-tag (SLAB0101, smart-lifesciences, China), anti-ANXA1 (T201086-5E4, Zen-bio, China), anti-PLIN4 (PH2286, Abmart, China), anti-ACACA (T55575, Abmart, China), anti-PCBP1 (T58059, Abmart, China), anti-LDHB (T58008, Abmart, China), anti-PCBP2 (T57300, Abmart, China), anti-CCT2 (T58449, Abmart, China), anti-LC3 I/II (F0144, Selleck, USA), anti-TCAB1 (sc-517078, Santa, USA), anti-GLI1 (TD7523, Abmart, China), anti-Cyclin D1 (30026ES50, Yeasen, China), anti-SNAIL (BD-PT4351, Biodragon, China), anti-ubiquitin (3936, CST, USA), anti-alpha-tublin (14555-1-AP, Proteintech, China).

RNA pull-down assay and mass spectrometry analysis

Biotin-labeled probes targeting circCLASP1 junction sites (RiboBio, Guangzhou, China) and oligo probes were used for RNA-protein pull-down assays (Pierce Magnetic RNA-Protein Pull-down Kit, Thermo Fisher, USA). Treated cell lysates were incubated with probe-bound streptavidin beads, and eluted RNA-binding protein complexes were analyzed by liquid chromatography-tandem mass spectrometry.

Ubiquitination assay

Cells were treated with MG132 (Sigma-Aldrich, USA) for 12 h, then harvested for IP with anti-GLI1 magnetic beads. Ubiquitin expression was detected by Western blot.

Cycloheximide (CHX) chase assay

MDA-MB-231 and MCF-7 cells were treated with 10 μg/ml CHX (Sigma-Aldrich, USA) for a time-course study. Protein samples generated from cell lysates were then performed with the Western blot analysis.

Dual-luciferase reporter assay

Dual luciferase reporter assay kit (TransGen Biotch, China) was utilized to detect the luciferase activity. Briefly, both MDA-MB-231 and MCF7 cell lines were cultured in 24-well culture plates and co-transfected with the corresponded plasmids mentioned below based on the required experiments: psiCHECK2-circCLASP1 WT and psiCHECK2-circCLASP1 MUT, together with the miR-15a-5p mimics or NC-mimics, respectively. After the incubation for 48 h, the Firefly luciferase activity and Renilla luciferase activity were detected by the fluorometer (FLx800, BioTek, USA).

Immunohistochemistry and immunofluorescence assay

Immunohistochemistry assays were performed using the Immunohistochemistry Kit (Yeasen, China). For immunofluorescence assays, the samples were sequentially processed as follows: fixed with acetone, washed with PBS, blocked with 10% goat serum, incubated with the antibodies, and finally mounted with DAPI-containing mounting medium. Images were captured under a microscope.

Coculture assays

Coculture systems were manipulated as previously described [15, 16].

Animal experiment

Female BALB/c nude (nu/nu) mice (6-week-old) were purchased from SPF Biotechnology (Beijing, China) and housed under SPF conditions. Mice were randomly divided into two groups and subcutaneously injected with MDA-MB-231 cells transfected with sh-circCLASP1-1 (1×10^7 cells/mouse) or sh-scramble as controls. For tail vein injection, a 1×10^5 cells/50 μL mixture was prepared and injected into 6-week-old BALB/c mice. After 3–4 weeks, mice were euthanized with CO_2, and lung tissues were collected. Animal experiments were approved by the Animal Use and Care Committee of China Agricultural University (No. AW62201202-3-8, AW21214202-3-07, and AW71705202-3-01).

Statistical analysis

GraphPad Prism 8 software and SPSS 26 software were used to analyze the experimental data. The eventual outcomes were represented as mean ± SD. Student's *t* test or ANOVA was conducted to illustrate the statistical significance, which was expressed by *P* value combined with asterisks (ns for no significance, $^*P \le 0.05$, $^{**}P \le 0.01$, and $^{***}P \le 0.001$).

RESULTS

CircCLASP1 is upregulated in BC tissues and serum

To identify the differentially expressed circRNAs in BC, we re-analyzed the RNA-seq dataset (GSE71651) and identified the top five most highly expressed circRNAs (Fig. 1A, B). To verify these findings, we performed reverse transcription-quantitative PCR (RT-qPCR) analyses in BC cell lines. Notably, we found that the expression level of circCLASP1 was the most significantly upregulated among these five circRNAs in BC cells (Fig. 1C). Based on these data, our research focused on circCLASP1.

CircCLASP1 (517 nucleotides) is formed by the reverse cleavage of exons 3–8 of its linear cognate *CLASP1* (cytoplasmic linker associated protein 1) (Fig. 1D). Using Sanger sequencing, we confirmed the presence of the back-splicing site (BSS) of circCLASP1 with PCR divergent primers in BC cells (Supplementary Fig. S1A). We further found that the target product of circCLASP1 could only be amplified by divergent primers from complementary DNA (cDNA) derived from BC cell lines, not from its genomic DNA (gDNA), indicating the existence of a BSS in the transcript (Supplementary Fig. S1B). To evaluate the association of circCLASP1 with clinical pathological characteristics, RT-qPCR was performed on tissue samples from BC patients ($n = 65$) and adjacent tissues ($n = 42$) (Fig. 1E). Analysis of clinicopathological characteristics revealed that circCLASP1 expression was positively associated with lymph node metastasis, ki67 expression, and tumor size (Supplementary Table S1). Notably, receiver operation characteristic (ROC) analysis demonstrated that circCLASP1 had an area under the curve (AUC) of 0.8196, with 100% specificity and 72.31% sensitivity. The 95% confidence interval (CI) was 0.7372–0.9020 (Fig. 1F). Additionally, we found that circCLASP1 was highly expressed in the serum of BC patients ($n = 61$) (Fig. 1G). ROC analysis showed an AUC of 0.8902, with 70% specificity and 96.72% sensitivity. The 95% CI was 0.7877–0.9926 (Fig. 1H). Using actinomycin D (ACTD), we found that circCLASP1 had a longer half-life than its linear cognate *CLASP1* in BC cells (Fig. 1I). Furthermore, we observed that the endogenous circCLASP1 resisted to RNase R digestion, while the linear *CLASP1* mRNA was notably digested by RNase R treatment (Supplementary Fig. S1C). Moreover, we noticed that circCLASP1 was mainly sub-located in the cytoplasm of cells (Fig. 1J).

CircCLASP1 knockdown attenuates growth, metastasis, and invasion of BC cells

To further explore the biological function of circCLASP1 in BC cells, we silenced the circCLASP1 expression by designing the short hairpin RNAs (shRNAs) to target the BSS of circCLASP1. We observed a significant reduction in circCLASP1 expression, while no significant alteration in the transcription of the linear *CLASP1* were noted in BC cells (Fig. 2A; Supplementary Fig. S2A). Multi-assay and statistical analyses (Fig. 2B, C; Supplementary Figs. S2B, C and S8A) demonstrated that circCLASP1 knockdown (sh-circCLASP1) attenuated the proliferative capacity and colony formation ability of BC cells. Consistently, immunofluorescence assays and statistical

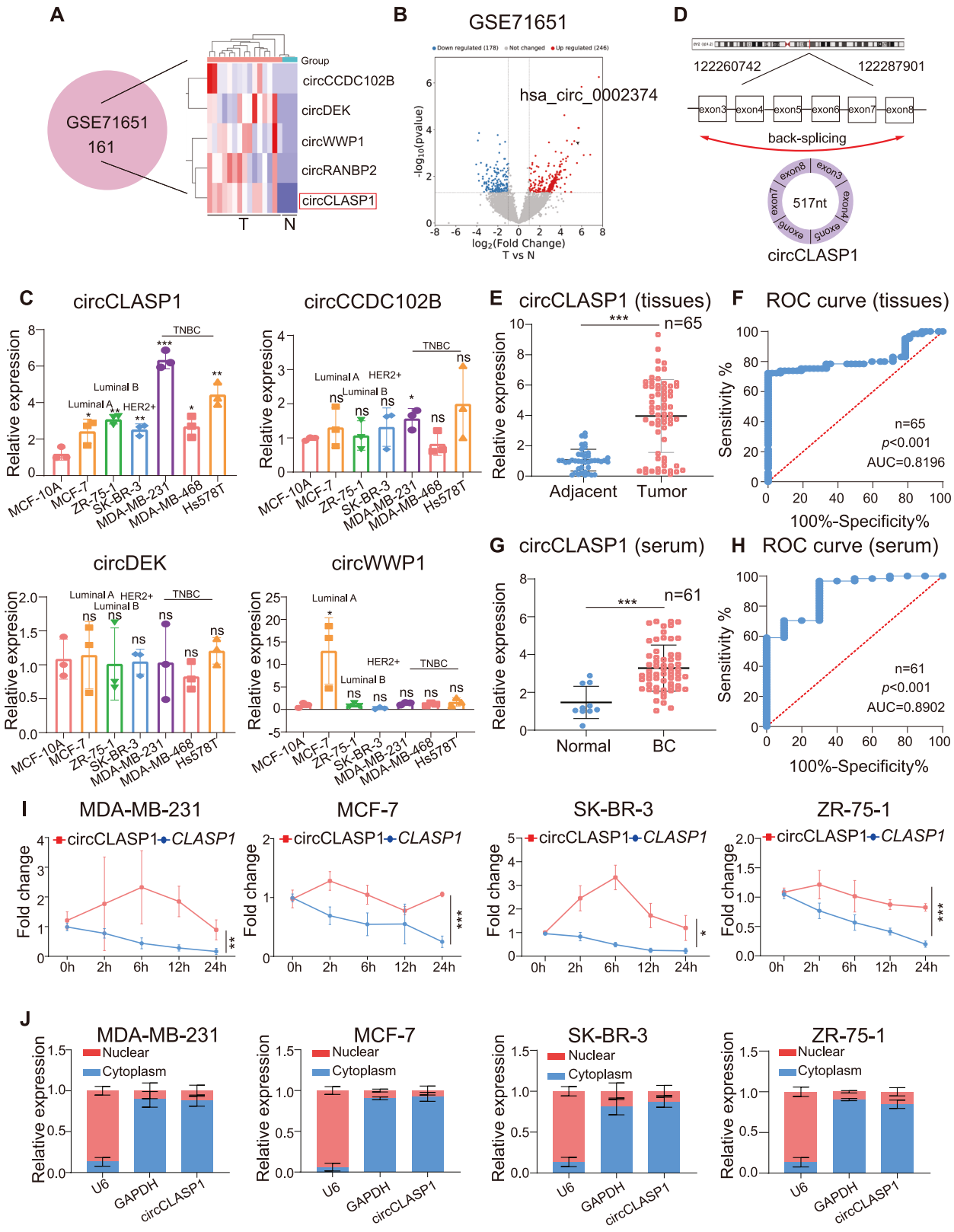

analyses (Fig. 2D; Supplementary Fig. S8B) showed that sh-circCLASP1 significantly inhibited ki67 expression in both MDA-MB-231 and MCF-7 cells. Moreover, using patient-derived organoid (PDO) from BC tissues, we observed slower growth and reduced organoid diameter in the sh-circCLASP1-PDO group compared to the sh-scramble-PDO control (Fig. 2E; Supplementary Fig. S8C). Subsequently, migration and invasion assays and statistical analyses (Fig. 2F; Supplementary Figs. S2D, S8D) revealed that the migratory and invasion abilities of the sh-circCLASP1 BC cell lines were notably reduced. Additionally, cell cycle analysis (Fig. 2G; Supplementary Fig. S2E) and cell distribution data (Supplementary Fig. S8E) showed that the sh-circCLASP1 MDA-MB-231 and MCF-7 cells

Fig. 1 Identification and characterization of circCLASP1 in BC. A Left: Differentially expressed circRNAs from the GSE71651 database; right: Top five upregulated circRNAs. N: Normal tissues ($n = 3$), T: Tumor tissues ($n = 15$). **B** Volcano plot showing differentially expressed circRNAs in GSE71651. **C** RT-qPCR analysis of circCCDC102B, circDEK, circWWP1, circCLASP1 in BC cell lines vs. normal epithelial cells (MCF-10A). CircRANBP2 lacks specific qPCR primers. $n = 3$. **D** Genomic mapping of circCLASP1. **E** CircCLASP1 expression in BC tissues ($n = 65$) vs. adjacent tissues ($n = 42$) as measured by RT-qPCR. **F** ROC curve evaluating the diagnostic potential of circCLASP1 in BC tissues. **G** CircCLASP1 expression levels in BC serum ($n = 61$) vs. normal serum ($n = 10$) as measured by RT-qPCR. **H** ROC curve assessing the diagnostic potential of circCLASP1 in BC serum. **I** RT-qPCR quantification of circCLASP1 and its linear counterpart *CLASP1* after ACTD treatment in BC cells. $n = 3$. **J** RNA nucleocytoplasmic separation of circCLASP1 in BC cells. *U6* and *GAPDH* served as nuclear and cytoplasmic markers, respectively. $n = 3$. Data are shown as the mean ± SD. $^{ns}p > 0.05$, $^{*}p \le 0.05$, $^{**}p \le 0.01$, $^{***}p \le 0.001$.

underwent cell cycle arrested. The number of apoptotic cells were increased in the sh-circCLASP1 BC cells (Fig. 2H; quantitative statistics in Supplementary Fig. S8F). Protein analysis revealed that the levels of BAX were elevated, while BCL2 levels were reduced in sh-circCLASP1 BC cells compared to the sh-scramble control group (Supplementary Fig. S2F).

To evaluate the biological functions of circCLASP1 in vivo, tumor-xenograft models were generated by injection of sh-scramble- or sh-circCLASP1- MDA-MB-231 cells into the BALB/c nude mice ($n = 5$/group), respectively. As expected, the weight of the tumor xenografts was decreased in the sh-circCLASP1 group compared to the vehicle control (Fig. 2I). We proved that sh-circCLASP1 suppressed the growth of BC both in vitro and in vivo.

U2AF2 promotes the biogenesis of circCLASP1

RBPs regulate the biogenesis of circRNAs by binding to their flank sequences [17]. Through integrative analysis using three RBP prediction datasets, we identified polypyrimidine tract binding protein 1 (PTBP1) and U2 small nuclear RNA auxiliary factor 2 (U2AF2) as the potential key upstream regulators involved in the biogenesis of circCLASP1 (Fig. 3A). Furthermore, gain-of-function experiments showed that overexpression of PTBP1 did not alter the level of circCLASP1, whereas overexpression of U2AF2 (OE-U2AF2) notably increased the expression of circCLASP1 (Fig. 3B; Supplementary Fig. S3A, B), suggesting the essential role of U2AF2 in regulating circCLASP1 biogenesis. Additionally, Western blot analysis revealed that U2AF2 expression was significantly elevated in BC tissues (Fig. 3C). Moreover, in lymph node-positive and ki67-positive BC patients, increased expression of U2AF2 was associated with a significantly reduced overall survival (OS) rate (Fig. 3D). This implicates that circCLASP1 may also be negatively correlated with the OS of BC patients. Consequently, we obtained a positive correlation between the expression of U2AF2 and its downstream circCLASP1 (Fig. 3E). These findings implied that circCLASP1 was also linked to the poor prognosis. Bioinformatic prediction using the circinteractome database revealed three potential binding sites of U2AF2 within the flanking sequence of circCLASP1 (Supplementary Fig. S3C). Subsequently, RIP assays with an anti-U2AF2 antibody confirmed that U2AF2 specifically binds to the '+112 ~ + 136' region of circCLASP1, rather than the '+863 ~ + 897' or '+175 ~ + 202' regions as indicated in Fig. 3F and Supplementary Fig. S3C. Finally, a series of rescue experiments demonstrated that OE-U2AF2 functionally enhanced the proliferation, migration, and invasion of BC cells, effects that were partially reversed by sh-circCLASP1 (Fig. 3G–I). Taken together, these results suggest that U2AF2 regulates circCLASP1 biogenesis by binding to a specific region in the flanking sequence of the *CLASP1* pre-mRNA.

CircCLASP1 promotes BC progression without acting as a sponge for miRNAs or neo-polypeptides

Previous studies have shown that circRNAs regulate the expression of their target genes by sponging miRNAs [18, 19]. By separating nuclear and cytoplasmic fractions from BC cells, we found that circCLASP1 was predominantly localized in the cytoplasm (Fig. 1H). Therefore, we hypothesized that circCLASP1 might function as a miRNA sponge in BC. In a RIP assay with an anti-AGO2 antibody, we observed that circCLASP1 fragments were significantly enriched in the AGO2-bound fraction (Fig. 4A), suggesting that circCLASP1 could potentially sponge miRNAs. To explore this further, we predicted miRNA candidates specific to circCLASP1 using multiple miRNA bioinformatics databases, and identified eleven potential miRNAs for initial analysis (Fig. 4B). Four of these miRNAs were selected for further investigation based on their relevance to clinical prognosis (Fig. 4C). In RNA pull-down assays, we found that miR-15a-5p was highly enriched by circCLASP1 probes (Fig. 4D). To confirm the interaction, we identified two putative miR-15a-5p binding sites on circCLASP1 through TargetScan prediction. We then constructed wild-type circCLASP1 (WT circCLASP1) and miRNA-binding site mutant circCLASP1 (2-site MUT circCLASP1) dual luciferase reporter plasmids. Dual luciferase assays showed that miR-15a-5p mimics significantly reduced the luciferase activity of the WT circCLASP1 reporter, but not the mutant circCLASP1 reporter (Fig. 4E). These results suggest that circCLASP1 can sponge miR-15a-5p.

However, in a series of rescue experiments, miR-15a-5p did not significantly inhibit BC progression in BC cells overexpressing circCLASP1 (OE-circCLASP1) (Fig. 4F–H). These findings indicate that circCLASP1 does not promote BC progression through sponging miR-15a-5p. Next, using the circRNADb database, we found that circCLASP1 has translational potential (Supplementary Fig. S4A). To verify this, we inserted a Flag-tag into the putative open reading frame of circCLASP1 without causing a frameshift mutation. However, immunoblotting results showed that no polypeptides were detected in cells expressing circCLASP1-FLAG, compared to the positive controls (Supplementary Fig. S4B).

CircCLASP1 functions as a molecular scaffold, binding to CCT2 and regulating the ubiquitin-mediated degradation of GLI1 in BC

RNA pull-down experiments were performed using two biotin-tagged probes for circCLASP1 (Fig. 5A). Seven protein candidates were identified via liquid chromatography-tandem mass spectrometry and selected for further validation (Score > 600) (Supplementary Fig. S5A). The binding capacity of these seven protein candidates to circCLASP1 was individually validated by Western blot. We observed that only chaperonin containing TCP1 subunit 2 (CCT2) could bind to circCLASP1 in both MDA-MB-231 and MCF-7 cells (Fig. 5B). Furthermore, circCLASP1 was co-precipitated with CCT2 in the lysate of BC cells using an anti-CCT2 antibody in RIP assays (Fig. 5C). Additionally, the binding of circCLASP1 to CCT2 was simulated using AlphaFold3 [20] (Fig. 5D).These results suggest that circCLASP1 binds to CCT2.

It has been reported that CCT2 has dual functions as both an autophagy receptor and a molecular chaperone [21]. To investigate the potential mechanism underlying the circCLASP1-CCT2 interaction, we performed a series of assays. First, through immunoblot analysis, we found that sh-circCLASP1 did not alter the protein level of the ATG8s family member (LC3) (Supplementary Fig. S5B). Second, when examining the protein levels of downstream targets of CCT2, such as TCAB1 and GLI1 [22, 23], we observed that the TCAB1 protein levels were unaffected in sh-circCLASP1 MDA-MB-231 and MCF-7 cells (Supplementary Fig. S5B). Immunoprecipitation assays revealed that sh-circCLASP1 weakened the interaction between CCT2 and GLI1 (Fig. 5E;

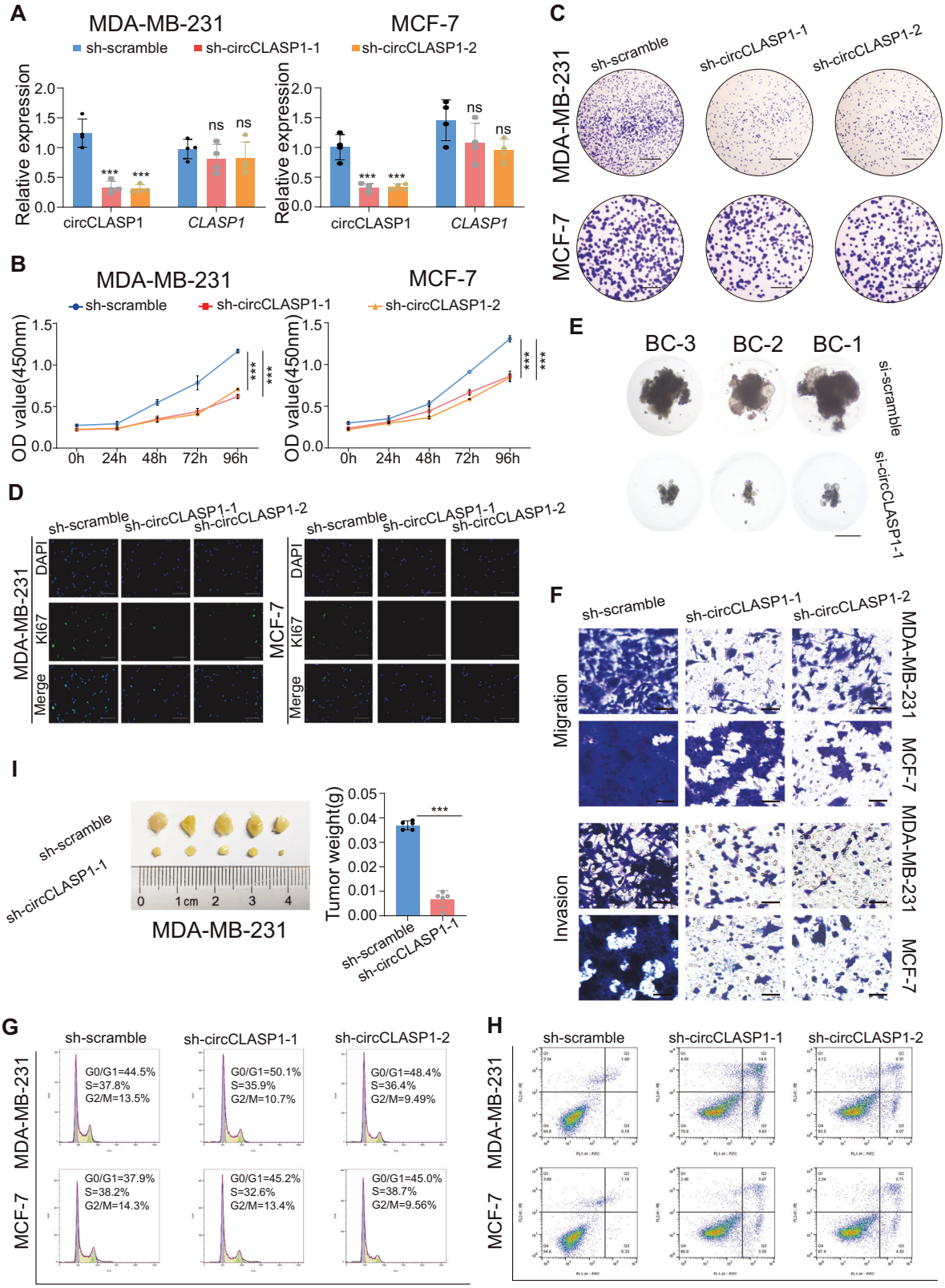

Supplementary Fig. S5C), suggesting that circCLASP1 may function as a molecular enhancer to facilitate the interaction between CCT2 and GLI1. Moreover, RIP assays using an anti-GLI1 antibody showed the presence of circCLASP1 in the complex, indicating an interactive network involving circCLASP1, CCT2, and GLI1 (Fig. 5F). Additionally, we found that circCLASP1 regulates the protein levels of GLI1, but not its mRNA (Supplementary Fig. S5D, E). Based on this observation, we hypothesized that circCLASP1 might help maintain the stability of GLI1. To test this, we used cycloheximide (CHX), a protein biosynthesis inhibitor, to evaluate the stability of GLI1. Compared to the sh-scramble groups, the sh-circCLASP1 groups showed significantly reduced stability of GLI1 protein in

Fig. 2 CircCLASP1 functions as an oncogene on BC cells. A Knockdown efficiency of circCLASP1 and its cognate linear transcript (*CLASP1*) detected by RT-qPCR in MDA-MB-231 and MCF-7 cells. $n = 4$. **B** CCK-8 assay showing the proliferation of MDA-MB-231 and MCF-7 cells transfected with sh-circCLASP1 or sh-scramble. $n = 3$. **C** Colony formation assay of MDA-MB-231 and MCF-7 transfected with sh-circCLASP1 or sh-scramble. Scale bar = 2 mm. **D** Representative immunofluorescence images of BC cells stained by ki67. Scale bar = 100 μm. **E** Representative images of BC patient-derived organoids (PDOs). Scale bar = 200 μm. **F** Transwell assay showing reduced migration and invasion in MDA-MB-231 and MCF-7 cells transfected with sh-circCLASP1. Scale bar = 100 μm. Flow cytometry analysis of cell cycle distribution (**G**) and apoptosis (**H**) in MDA-MB-231 and MCF-7 with sh-circCLASP1 or sh-scramble. **I** Left: BALB/c nude mice ($n = 5$ per group) were injected with MDA-MB-231 cells transfected with sh-circCLASP1-1 or sh-scramble. Right: Xenograft weights were recorded. Data are shown as the mean ± SD. $^{ns}p > 0.05$, $^{***}p \leq 0.001$.

both MDA-MB-231 and MCF-7 cells (Fig. 5G; Supplementary Fig. S5F). Since the ubiquitin-proteasome system is the primary pathway responsible for intracellular protein degradation [24], we treated the cells with MG132 (a proteasome inhibitor). The results indicated that the decrease in GLI1 protein levels caused by sh-circCLASP1 was prevented in MG132-treated MDA-MB-231 and MCF-7 cells (Fig. 5H). Additionally, we observed reduced GLI1 protein levels and increased GLI1 ubiquitination in the sh-circCLASP1 groups in both MDA-MB-231 and MCF-7 cells (Fig. 5I). These findings suggest that circCLASP1 binds to CCT2 and regulates the stability of GLI1 in a ubiquitination-dependent manner.

CircCLASP1 regulates *SNAIL* expression through GLI1 in BC

It has been suggested that GLI1 is an essential transcription factor [25] that promotes the progression of BC [26–28]. To investigate the role of circCLASP1 in regulating GLI1, we performed immunocytochemistry assays and nucleus-cytoplasm separation analyses. We observed that sh-circCLASP1 inhibited the nuclear accumulation of GLI1 in BC cells (Fig. 6A, B). These results suggest that circCLASP1 regulates the transcriptional activity of GLI1. We next analyzed the survival curves of the downstream target genes of GLI1 and found that BC patients with increased SNAIL expression had significantly worse OS (Fig. 6C). Our data also indicated that GLI1 and SNAIL were highly expressed in BC cell lines (Fig. 6D). In a cohort of 1 100 BC patients, we observed a significant positive correlation between GLI1 and SNAIL expression, suggesting that the GLI1/SNAIL axis plays a role in BC progression (Fig. 6E). Moreover, sh-circCLASP1 treatment markedly reduced both mRNA and protein levels of SNAIL in BC cells (Fig. 6F, G). Consistently, tumor samples from an independent cohort of 65 BC patients also exhibited a significant positive correlation between circCLASP1 and SNAIL expression (Fig. 6H). These findings suggest that circCLASP1 regulates the GLI1/SNAIL axis in BC.

To investigate the functional roles of circCLASP1, we overexpressed either WT circCLASP1 or 2-site MUT circCLASP1 in BC cells. Both WT and 2-site MUT circCLASP1 significantly enhanced cell proliferation (Supplementary Fig. S6A), colony formation (Supplementary Fig. S6B), and migratory and invasive capacities (Supplementary Fig. S6C), indicating that the oncogenic function of circCLASP1 is retained even when miRNA binding is disrupted. To elucidate the underlying molecular mechanism, we further examined the interaction between CCT2 and GLI1 proteins in BC cells overexpressing WT or 2-site MUT circCLASP1 (Supplementary Fig. S6D). The results demonstrated that the CCT2–GLI1 interaction was not affected by the 2-site MUT circCLASP1. Moreover, overexpression of 2-site MUT circCLASP1 also upregulated SNAIL expression (Supplementary Fig. S6E). These findings suggest that circCLASP1 exerts its oncogenic effects predominantly through the CCT2/GLI1/SNAIL axis in a miR-15a-5p-independent manner.

CircCLASP1 enhances macrophage recruitment and promotes lung metastasis through SNAIL in BC

TME plays a crucial role in BC progression, with T cells and macrophages being particularly important [11]. To explore whether circCLASP1 mediates the TME, we analyzed T cells and macrophages in cancer tissues. Immunohistochemistry staining revealed that patients with low circCLASP1 expression had fewer CD68-positive cells, while there was no difference in CD3-positive cells between samples with high or low circCLASP1 expression (Fig. 7A, B). These results imply that circCLASP1 might mediate the macrophage immunobiology in BC. To further investigate the involvement of circCLASP1 in BC macrophage immunobiology, we established an in vitro co-culture system using conditioned medium from BC cell lines. Gain- or loss-of-function assays indicated that co-culturing with conditioned medium from OE-circCLASP1-MDA-MB-231 cells inhibited the polarization of M0-like macrophages to M2-like macrophages. Conversely, this polarization was enhanced when THP-1 cells were supplied with conditioned medium from OE-circCLASP1-MCF-7 cells (Fig. 7C). Moreover, we detected the mRNA levels of *CCL2* and *CCL5*, which promote the recruitment of tumor-associated macrophages [29, 30], in sh-circCLASP1-MDA-MB-231 and OE-circCLASP1-MCF-7 cells. RT-qPCR results showed that sh-circCLASP1 significantly reduced the mRNA levels of *CCL2* and *CCL5* in MDA-MB-231 cells, while OE-circCLASP1 had the opposite effect in MCF-7 cells (Fig. 7D). Next, we constructed a circCLASP1 overexpression vector with an EGFP tag and stably transfected it into MCF-7 cells (Supplementary Fig. S7A), which were then co-cultured with macrophages. The recruitment of macrophages was monitored in real-time. Notably, cells with OE-circCLASP1-EGFP significantly recruited macrophages (Fig. 7E; Supplementary Video S1, 2). Furthermore, sh-circCLASP1-MDA-MB-231 cells indirectly co-culture with THP1 inhibited the migration of THP-1 cells, whereas OE-circCLASP1-MCF-7 cells promoted their migration (Fig. 7F). These results suggest that circCLASP1 mediates the recruitment of macrophages in BC. Previous studies have indicated that SNAIL regulates macrophage recruitment and tumor progression [16]. To investigate whether circCLASP1 mediates BC progression via SNAIL in vivo, we performed rescue experiments using 4T1 cells in a mouse tail vein injection model of lung metastasis (Fig. 8A). Notably, circCLASP1 is highly conserved between humans and mice (Supplementary Fig. S7B), supporting the translational relevance of this model. The results demonstrated that OE-circClasp1 promoted lung metastasis (Fig. 8B, C, E, G, I, K), upregulated Snail expression (Fig. 8D, H), enhanced macrophage recruitment (Fig. 8F, G, J, K), whereas sh-Snail reversed these effects. These findings suggest that circCLASP1 mediates macrophage recruitment to promote tumor metastasis through SNAIL in BC.

DISCUSSION

In recent years, both the incidence and mortality of female BC have been increasing [1], and it is particularly important to identify effective therapeutic targets and biomarkers. Recently studies have increasingly confirmed the multiple regulatory roles of circRNAs in cancer progression. Hereon, we report the oncogenic effect of circCLASP1 on BC progression using clinical samples, PDOs, xenograft mouse models, and BC cell lines. Moreover, we demonstrate that RBP-U2AF2 mediates the biogenesis of circCLASP1 by binding to its flanking sequence. Mechanistically, circCLASP1 functions as a protein scaffold by interacting with CCT2 to regulate the ubiquitination of GLI1 and the GLI1/SNAIL axis. Furthermore, we show that circCLASP1 enhances macrophage migration and promotes BC metastasis.

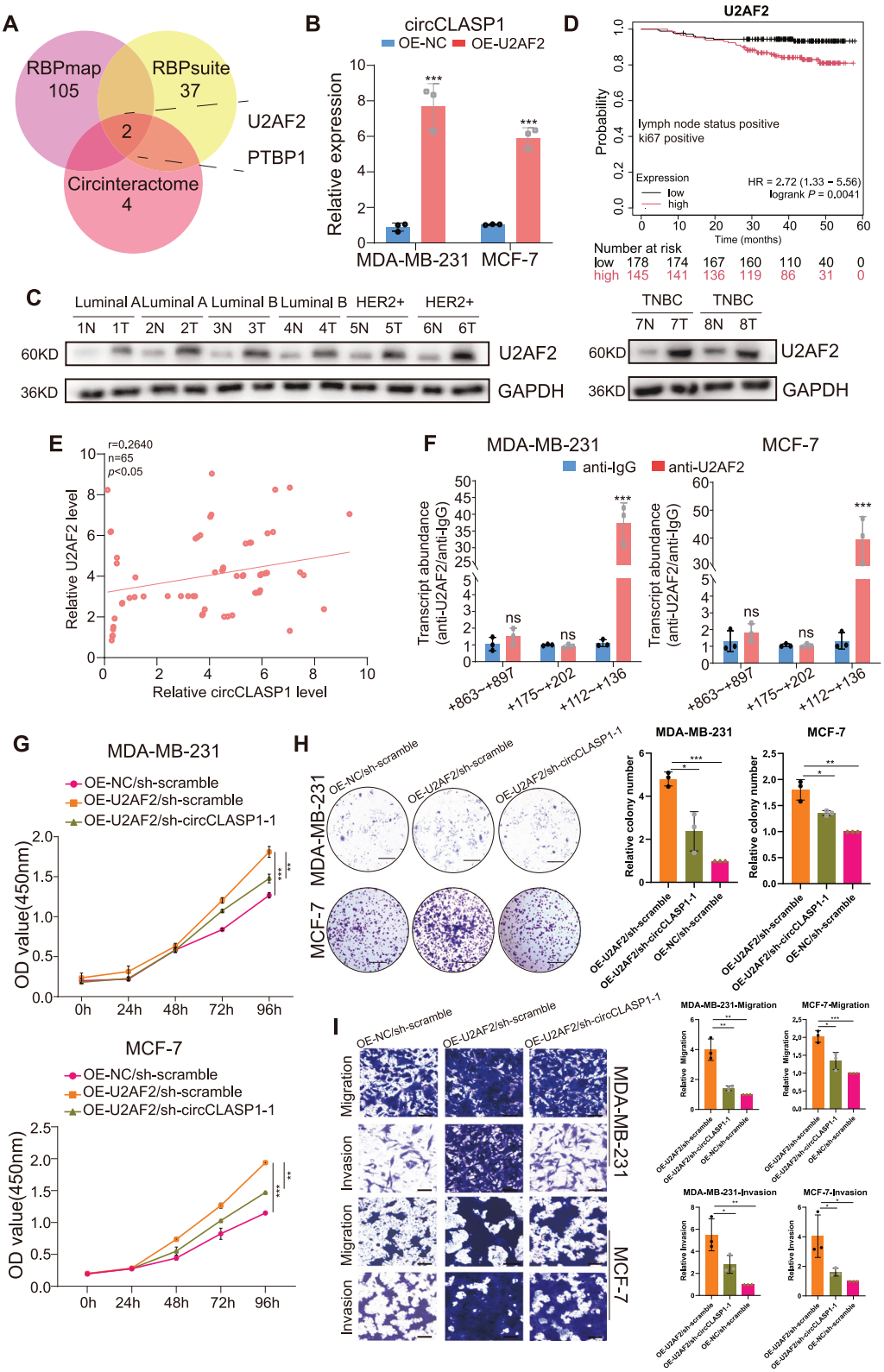

Fig. 3 U2AF2 mediates the biogenesis of circCLASP1. A Putative RBPs involved in circCLASP1 biogenesis were screened using RBPmap, RBPsuite, and circinteractome. **B** CircCLASP1 expression is regulated by OE-U2AF2. **C** U2AF2 protein levels in BC tissues (N: adjacent tissues, $n = 8$; T: tumor tissues, $n = 8$). **D** Kaplan–Meier survival analysis of U2AF2 expression in BC tissues ($n = 323$). **E** Correlation between U2AF2 and circCLASP1 in BC tissues ($n = 65$). **F** RIP assays confirming U2AF2 binding to circCLASP1 flanking sequences in MDA-MB-231 and MCF-7. $n = 3$. **G–I** Functional assays in MDA-MB-231 and MCF-7 cells transfected with sh-scramble or sh-circCLASP1-1, followed by OE-NC or OE-U2AF2: **G** CCK-8 proliferation assay. $n = 3$. **H** Left: Colony formation assay (MDA-MB-231, scale bar = 500 μm; MCF-7, scale bar = 2 mm). Right: Quantification of colony formation. $n = 3$. **I** Left: Transwell migration and invasion assay (scale bar = 100 μm). Right: Quantification of migration and invasion. $n = 3$. Data are shown as the mean ± SD. $^{ns}p > 0.05$, $^{*}p \le 0.05$, $^{**}p \le 0.01$, $^{***}p \le 0.001$.

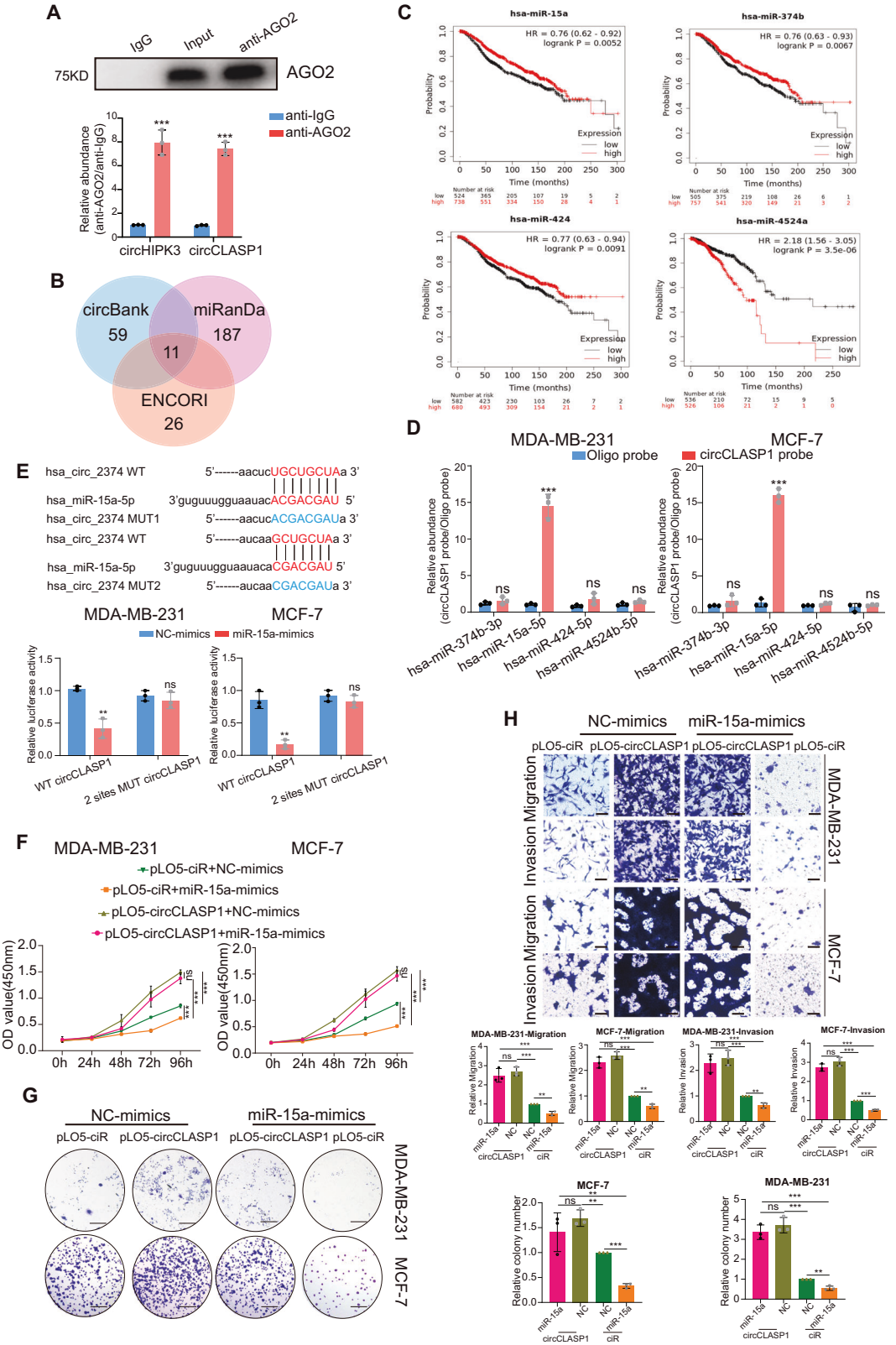

Fig. 4 CircCLASP1 promotes BC progression without acting as a sponge for miRNAs. A Upper: RIP with an anti-AGO2 antibody. Lower: RT-qPCR analysis of circCLASP1 levels, with circHIPK3 as an internal positive control. $n = 3$. **B** Predicted miRNAs binding to circCLASP1 based on circBank, miRanda, and ENCORI databases. **C** Kaplan–Meier analysis of miRNAs in BC. **D** RNA pull-down assays using circCLASP1 probes to identify its target miRNAs. $n = 3$. **E** Upper: Binding prediction between miR-15a-5p and circCLASP1. Lower: Dual-luciferase reporter assays validating circCLASP1-miR-15a-5p in MDA-MB-231 and MCF-7. $n = 3$. **F–H** Functional assays of miR-15a-5p on BC cells: **F** cell proliferation, $n = 3$. **G** Left: colony formation (MDA-MB-231, scale bar = 500 μm; MCF-7, scale bar = 2 mm). Right: Quantification of colony formation. $n = 3$. **H** Upper: Transwell assays (scale bar = 100 μm) after co-transfection of miR-15a-5p mimics and pLO5-circCLASP1. Lower: Quantification of migration and invasion. $n = 3$. Data are shown as the mean ± SD. $^{ns}p > 0.05$, $^{*}p \le 0.05$, $^{**}p \le 0.01$, $^{***}p \le 0.001$.

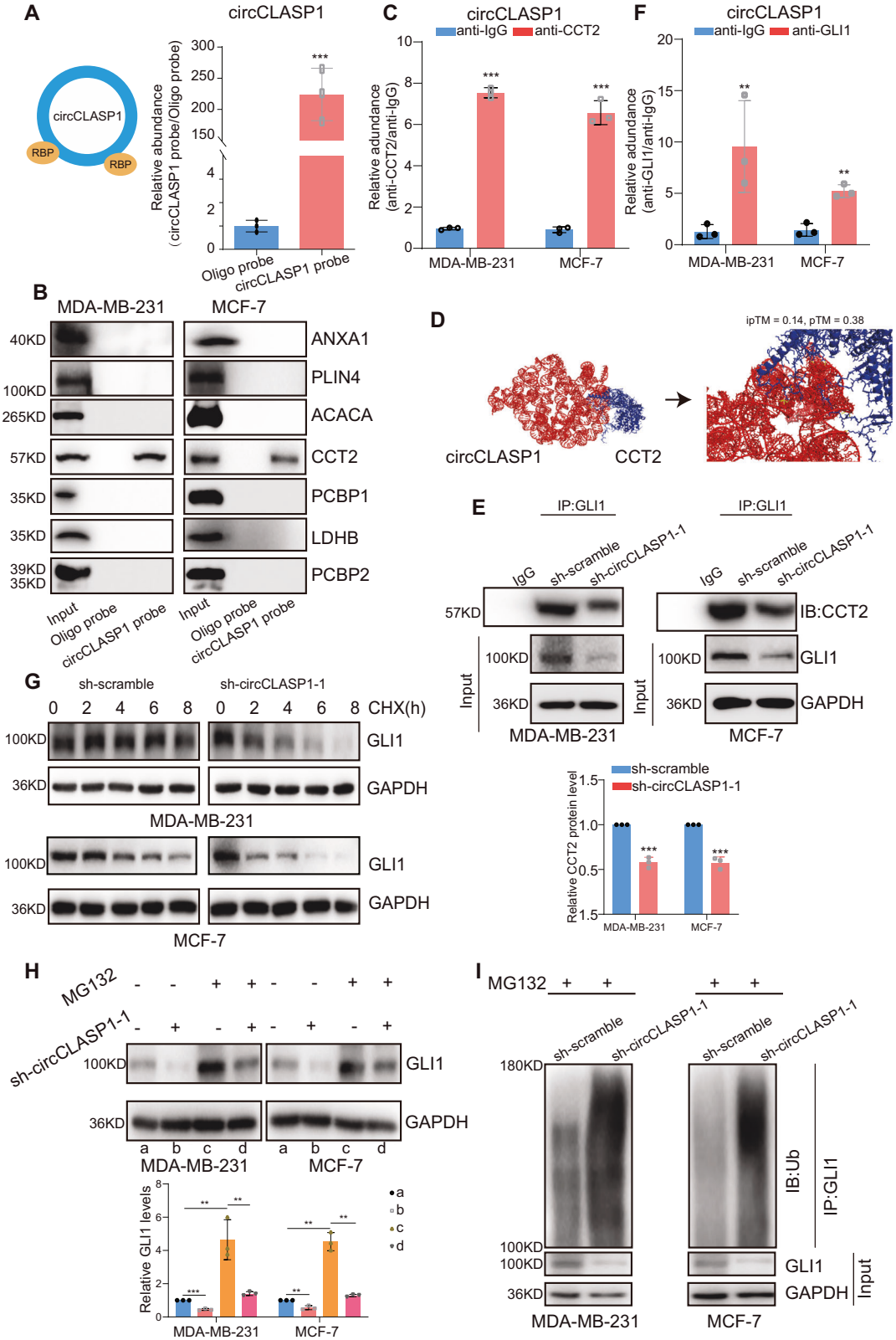

Through integrative analysis, we identified that circCLASP1 is upregulated in BC. Experimentally, we confirmed that its high expression in multiple BC cell lines, BC tissues ($n = 65$), and BC serum ($n = 61$). ROC analysis revealed that circCLASP1 exhibited AUC values of 0.8196 and 0.8902, respectively. We demonstrated that sh-circCLASP1 inhibited the proliferation and metastasis of BC cell lines. Notably, we showed that sh-circCLASP1 significantly slowed the growth of BC PDOs compared to sh-scramble PDOs. Additionally, circCLASP1 was found to mediate the recruitment of macrophages and induce M2-like macrophage polarization, influencing the BC TME. In vivo experiments further supported the role of circCLASP1 in promoting BC tumor growth and

Fig. 5 CircCLASP1 binds to CCT2 and regulates the ubiquitin-mediated degradation of GLI1. A Left: Schematic representation of circRNA-protein binding. Right: Enrichment of circCLASP1-specific probes detected by RT-qPCR. $n = 3$. **B** RNA pull-down and Western blot assays assessing circCLASP1 binding to seven candidate proteins. **C** RIP using anti-CCT2 antibody validating CCT2 binding to circCLASP1. $n = 3$. **D** Three-dimensional simulated structure of the circCLASP1-CCT2 interaction, with the binding site highlighted in yellow. **E** Upper: IP using anti-GLI1 antibody detecting GLI1-CCT2 interaction in sh-circCLASP1- MDA-MB-231 and MCF-7 cells. Lower: Quantification of CCT2 protein levels using ImageJ. $n = 3$. **F** RIP with anti-GLI1 antibody assessing GLI1 enrichment on circCLASP1 in MDA-MB-231 and MCF-7 cells. $n = 3$. **G** Western blot of CHX-treated samples assessing the half-life of GLI1 in sh-circCLASP1-1 vs. sh-scramble. **H** Upper: Western blot analysis of MG132-treated samples showing GLI1 degradation. Lower: Quantification of GLI1 protein levels using ImageJ. $n = 3$. **I** Ubiquitination levels of GLI1 detected in sh-circCLASP1-1 transfected MDA-MB-231 and MCF-7 cells. Data are shown as the mean ± SD. $^{**}p \le 0.01$, $^{***}p \le 0.001$.

facilitating lung metastasis. Importantly, to explore the potential of circCLASP1 as a diagnostic biomarker or therapeutic target, large-scale clinical studies in BC patients are warranted.

RBPs are currently considered crucial regulators of circRNA biogenesis [31]. Emerging studies have indicated that various RBPs, including FUS, QKI, and EIF4A3 are involved in the generation of numerous cirRNAs and influence the progression of cancer [17, 32–35]. In our study, we identified that U2AF2 could bind to the '+112~+136' region located in the flanking sequence of circCLASP1 and significantly promoted its biogenesis. Furthermore, we observed that higher U2AF2 expression was associated with shorter OS rate in lymph node-positive and ki67-positive BC patients. Additionally, our findings demonstrated that the U2AF2 expression was positively correlated with circCLASP1 expression in BC. Moreover, a series of rescue experiments systematically showed that the attenuated phenotypes (proliferation, migration, and invasion) in sh-circCLASP1 BC cells were significantly rescued by OE-U2AF2. These results suggest that the endogenous production of circCLASP1 is regulated by U2AF2.

Using RNA pull-down and MS analysis, we confirmed that CCT2 specifically bound to circCLASP1 among the other candidates. CCT2, a molecular chaperone and autophagy receptor [21–23, 36, 37], plays crucial roles in protein folding and stabilization. It assists in folding TCAB1 to regulate telomerase activity [22] and stabilizes GLI1 to promote colorectal cancer [23], while also facilitating the clearance of protein aggregates [21, 38]. In our study, we found that sh-circCLASP1 did not affect the protein levels of TCAB1 and LC3, but it significantly decreased the levels of GLI1 protein, without altering its mRNA expression. Moreover, GLI1 was highly expressed in various BC cell lines, and circCLASP1 regulated GLI1 stability via the ubiquitin-proteasome system, promoting its nuclear accumulation. Previous studies suggested GLI1 primarily functions as a transcription factor to drive BC progression [26, 27, 39, 40]. Notably, we further analyzed the OS of its downstream genes and found that SNAIL exhibited the most significant difference in OS. Furthermore, circCLASP1 expression was positively correlated with SNAIL levels.

Previous studies have shown that most circRNAs sponge miRNAs to perform their functions [7], we confirmed the interaction between circCLASP1 and miR-15a-5p using RIP, RNA pull-down, and dual-luciferase assays. Although miR-15a-5p exhibited strong tumor-suppressive effects in BC cells, its overexpression failed to rescue circCLASP1-induced oncogenic phenotypes. Moreover, mutating miR-15a-5p binding sites on circCLASP1 did not diminish its tumor-promoting effects. IP-Western blot further demonstrated that circCLASP1 enhanced CCT2-GLI1 interaction and upregulated SNAIL expression, regardless of miR-15a-5p binding. These results suggest that circCLASP1's oncogenic role in BC is primarily mediated through the CCT2/GLI1/SNAIL/CCL2-CCL5 axis, independent of miR-15a-5p sponging.

Cancer immunotherapy has revolutionized treatment by targeting the TME [41, 42], yet its efficacy remains limited in many patients due to poorly understood immune microenvironment mechanisms [43, 44]. Therefore, elucidating TME heterogeneity in BC is essential for advancing immunotherapy. In our study, we found that sh-circCLASP1 weakened the interaction between CCT2 and GLI1, promoting GLI1 ubiquitination and suppressing its transcriptional activity, ultimately reducing SNAIL expression. Moreover, overexpression of circCLASP1 upregulates the expressions of CCL2 and CCL5 in BC cells, consequently enhancing macrophage migration and recruitment. It is well known that CCL2 predominantly facilitates TAM infiltration in BC, and together with CCL5, these chemokines substantially reshape the surrounding TME [29, 30]. Both CCL2 and CCL5 primarily exert their functions through their receptors-CCL2/CCR2, CCL5/CCR5, and CCL5/CCR3 [45–47]. Single-cell RNA sequencing data of BC show that CCR2 is predominantly expressed in myeloid cells, T cells, and plasmablasts, while CCR5 is mainly expressed in myeloid cells and T cells. In contrast, CCR3 expression is relatively low across BC cell types [48]. Notably, macrophage represents a major subset of myeloid cells [48]. Within the TME, T cells and macrophages are most prominent, while other immune cell types are less abundant in BC [11]. In line with these results, a greater reduction in $CD68^+$ than in $CD3^+$ cells were observed in the circCLASP1 low-expression group of human BC tissues, suggesting that TAMs—rather than T cells—are the predominant mediators in the circCLASP1/GLI1/SNAIL/CCL2–CCL5 regulatory axis within the TME of BC.

In BC, the elevated expressions of CCL2 and CCL5 drive substantial infiltration of TAMs (predominantly M2-polarized and pro-tumoral) [16]. In agreement, we found that circCLASP1-overexpressed BC cells not only recruit TAMs via increased CCL2 and CCL5 expression but also induce macrophages to adopt an M2-like phenotype. This high abundance of M2-TAMs profoundly remodels TME, exerting extensive effects on other cellular components: TAM-secreted immunosuppressive factors (e.g., IL-8, TGF-β, PGE2) recruit and activate other myeloid-derived suppressor cells (MDSCs), which potently suppress the anti-tumor activity and proliferation of $CD8^+$ T cells and natural killer (NK) cells [49–52]. Concurrently, they promote the recruitment, expansion, and functional enhancement of regulatory T cells (Tregs), further inhibiting effector T-cell responses [53].

Furthermore, TAMs interact with cancer cells to stimulate adjacent fibroblast activation into cancer-associated fibroblasts (CAFs) through the release of factors such as TGF-β and PDGF [54]. Activated CAFs in turn feedback by secreting additional CCL2/CCL5 and other pro-inflammatory/angiogenic factors (e.g., VEGF, IL-6), establishing a vicious cycle that promotes angiogenesis, extracellular matrix remodeling, and tumor invasion/metastasis [12, 55–57]. Ultimately, this CCL2/CCL5-TAM axis may orchestrate a TME characterized by potent immunosuppression, tumor progression, and immune evasion.

Although this study focused on macrophage-centric mechanisms, the potential role of other immunosuppressive cell types or stromal components deserves further investigation in a large multicenter clinical sample of BC and deeper molecular action.

Despite significant progress in BC treatment, post-operative recurrence and metastasis remain the primary causes of cancer-related mortality. Thus, there is an urgent need for more precise and effective predictive biomarkers to guide clinical management and improve patient prognosis. Our study found that circCLASP1 expression was correlated with lymph node metastasis, ki67 expression, and tumor size in tumor tissues of BC patients ($n = 65$), with an AUC of 0.8196 (Fig. 1F; Supplementary Table S1).

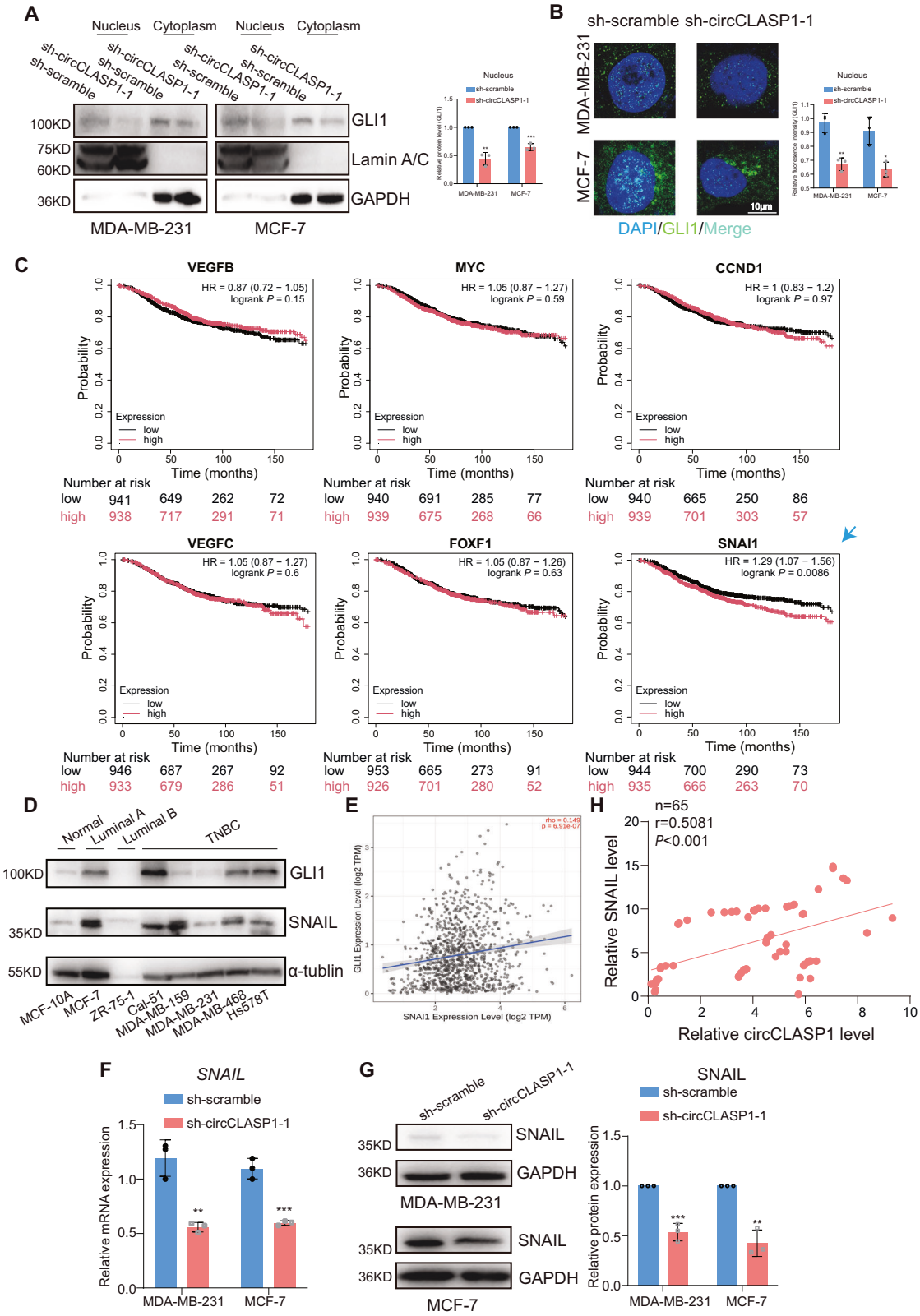

Fig. 6 CircCLASP1 regulates *SNAIL* expression at the transcriptional level through GLI1. Western blot (**A**) and immunofluorescence staining (**B**) assays were used to examine the effect of circCLASP1 on the nuclear accumulation of the GLI1 protein in MDA-MB-231 and MCF-7 cells. $n = 3$. **C** Kaplan–Meier analysis of VEGFB, MYC, CCND1, VEGFC, FOXF1, SNAI1 (SNAIL) in BC patients. **D** Western blot analysis of GLI1 and SNAIL protein levels in BC cell lines. **E** Correlation analysis of GLI1 and SNAIL in a BC cohort ($n = 1\,100$). mRNA (**F**) and protein (**G**) expression levels of SNAIL in sh-circCLASP1-1 transfected MDA-MB-231 and MCF-7 cells. $n = 3$. **H** Correlation analysis between circCLASP1 and *SNAIL* expression in BC tissues ($n = 65$). Data are shown as the mean ± SD. *$p \le 0.05$, **$p \le 0.01$, ***$p \le 0.001$.

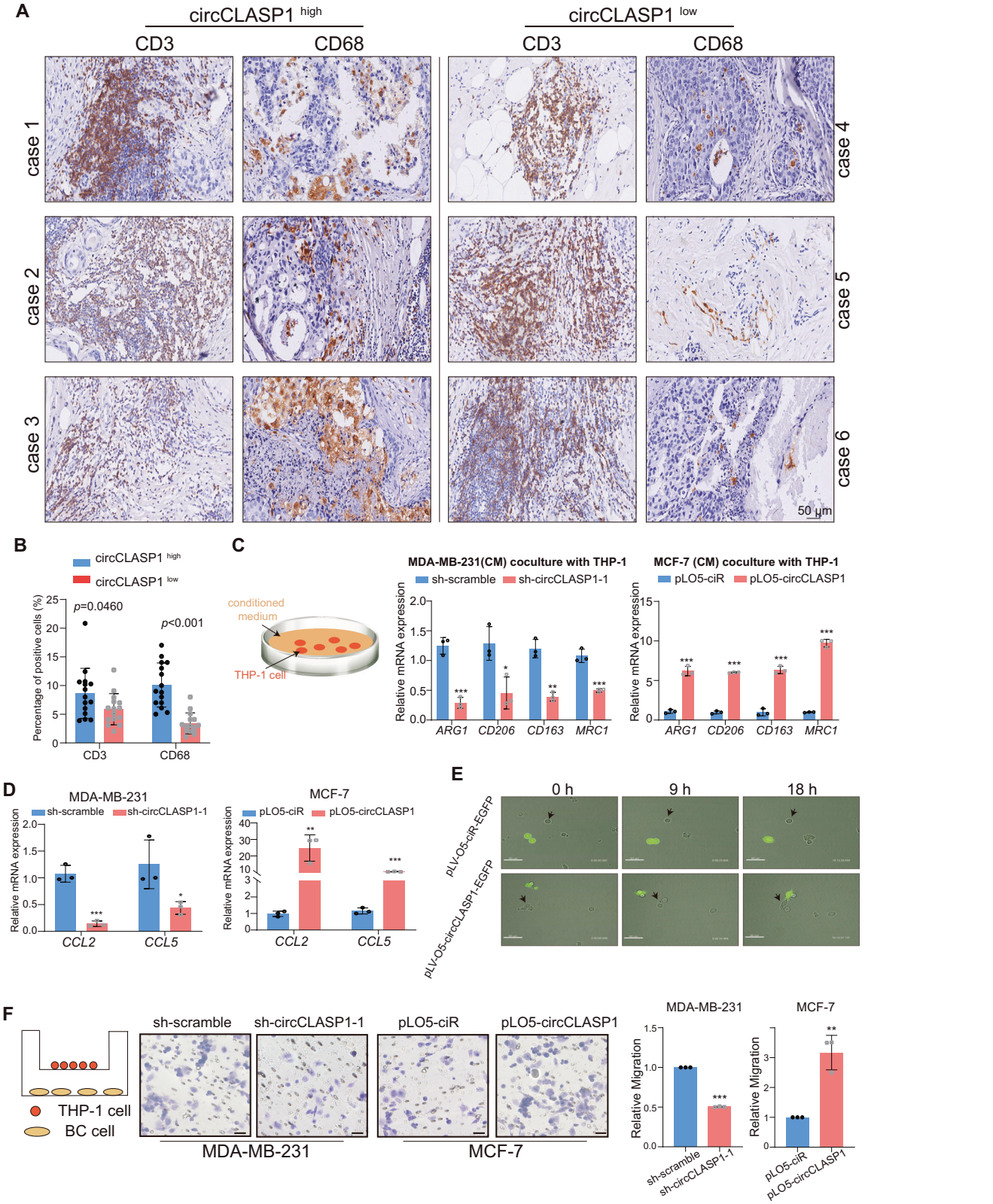

Fig. 7 CircCLASP1 enhances macrophage recruitment in BC cells. A Immunohistochemistry analysis of CD3 and CD68 in BC tissues with high or low circCLASP1 expression (scale bar = 50 μm). **B** Quantification of the proportion of $CD3^+$ and $CD68^+$ cells. $n = 15$. **C** Left: Schematic diagram illustrating the co-culture of conditioned medium (CM) with THP-1 cells. Right: mRNA expression levels of M2-like macrophage markers detected by RT-qPCR. $n = 3$. **D** Relative mRNA expression levels of *CCL2* and *CCL5* detected by RT-qPCR in MDA-MB-231 and MCF-7 cells. $n = 3$. **E** Images of OE-circCLASP1-EGFP MCF7 directly co-culture with M0-like THP-1 at 0 h, 9 h, and 18 h. Scale bar = 50 μm. **F** Left: Migration assay of THP-1 cells indirectly co-cultured with BC cells (scale bar = 100 μm). Right: Quantification of migration. $n = 3$. Data are shown as the mean ± SD. $^*p \le 0.05$, $^{**}p \le 0.01$, $^{***}p \le 0.001$.

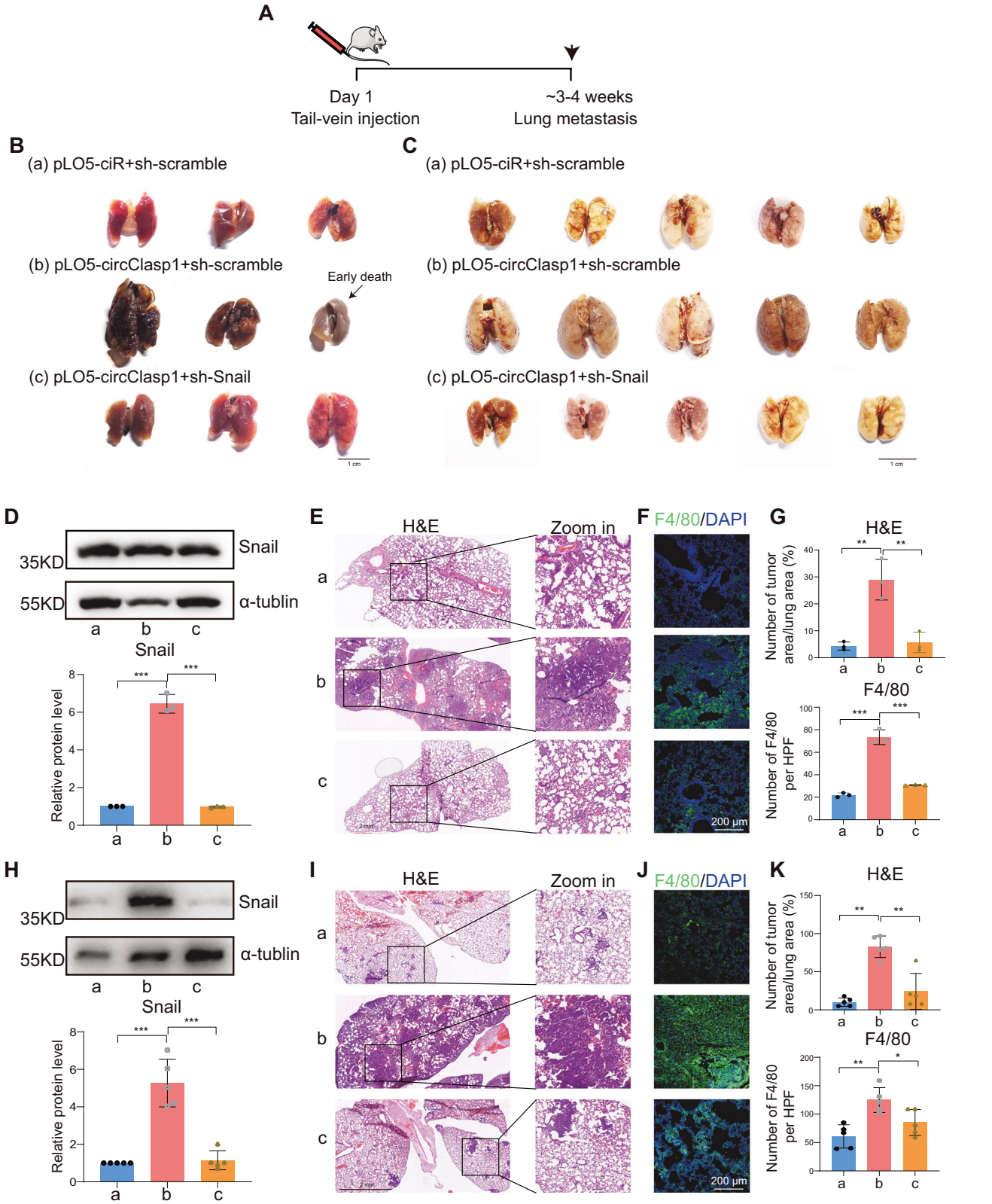

Fig. 8 CircClasp1 promotes lung metastasis through Snail in vivo. A Schematic representation of tail-vein injection in mice. **B**, **C** Lung metastasis foci (scale bar = 1 cm) in a metastasis model induced by OE-circClasp1 and sh-Snail 4T1 cells. **B** $n = 3$. **C** $n = 5$. **D**, **H** Upper: Western blot analysis of Snail protein levels in mouse lung tissues. Lower: Quantification of Snail protein levels using ImageJ. **D** $n = 3$. H, $n = 5$. **E**, **I** Representative H&E staining of lung sections (scale bar = 2 mm). **E** $n = 3$. **I** $n = 5$. **F**, **J** Representative immunofluorescence staining of F4/80 and DAPI (scale bar = 200 μm). **F** $n = 3$. **J** $n = 5$. **G**, **K** Upper: Quantification of metastatic area percentage. Lower: F4/80-positive cells per high-power field (HPF). **G** $n = 3$. **K** $n = 5$. Data are shown as the mean ± SD. $^{*}p \le 0.05$, $^{**}p \le 0.01$, $^{***}p \le 0.001$.

Furthermore, circCLASP1 could also be detected in the serum of BC patients ($n = 61$), showing an AUC of 0.8902 (Fig. 1H), suggesting its potential as a biomarker. To confirm its clinical applicability, further validation must be performed in multicenter, large sample independent cohorts, either as a standalone marker or in combination with other established biomarkers. Elucidating the functional impact and molecular mechanisms underlying circCLASP1's protein-binding capabilities will offer valuable insights into its role in tumorigenesis and support the development of novel therapeutic strategies.

In summary, this study integrates functional validation with clinical evidence to demonstrate that circCLASP1 is a key regulator of BC progression.

DATA AVAILABILITY

All data included in this study are available upon request by contact with the corresponding author.

REFERENCES

1. Bray F, Laversanne M, Sung H, Ferlay J, Siegel RL, Soerjomataram I, et al. Global cancer statistics 2022: GLOBOCAN estimates of incidence and mortality worldwide for 36 cancers in 185 countries. CA Cancer J Clin. 2024;74:229–63.
2. Harbeck N, Gnant M. Breast cancer. Lancet. 2017;389:1134–50.
3. Samuel SM, Varghese E, Varghese S, Busselberg D. Challenges and perspectives in the treatment of diabetes associated breast cancer. Cancer Treat Rev. 2018;70:98–111.
4. Zeng X, Liu C, Yao J, Wan H, Wan G, Li Y, et al. Breast cancer stem cells, heterogeneity, targeting therapies and therapeutic implications. Pharmacol Res. 2021;163:105320.
5. Harbeck N, Salem M, Nitz U, Gluz O, Liedtke C. Personalized treatment of early-stage breast cancer: present concepts and future directions. Cancer Treat Rev. 2010;36:584–94.
6. Kristensen LS, Jakobsen T, Hager H, Kjems J. The emerging roles of circRNAs in cancer and oncology. Nature reviews. Clin Oncol. 2022;19:188–206.
7. Kristensen LS, Andersen MS, Stagsted LVW, Ebbesen KK, Hansen TB, Kjems J. The biogenesis, biology and characterization of circular RNAs. Nat Rev Genet. 2019;20:675–91.
8. Li P, Song R, Yin F, Liu M, Liu H, Ma S, et al. circMRPS35 promotes malignant progression and cisplatin resistance in hepatocellular carcinoma. Mol Ther J Am Soc Gene Ther. 2022;30:431–47.
9. Song R, Ma S, Xu J, Ren X, Guo P, Liu H, et al. A novel polypeptide encoded by the circular RNA ZKSCAN1 suppresses HCC via degradation of mTOR. Mol Cancer. 2023;22:16.
10. Song R, Guo P, Ren X, Zhou L, Li P, Rahman NA, et al. A novel polypeptide CAPG-171aa encoded by circCAPG plays a critical role in triple-negative breast cancer. Mol Cancer. 2023;22:104.
11. Harris MA, Savas P, Virassamy B, O'Malley MMR, Kay J, Mueller SN, et al. Towards targeting the breast cancer immune microenvironment. Nat Rev Cancer. 2024;24:554–77.
12. Costa A, Kieffer Y, Scholer-Dahirel A, Pelon F, Bourachot B, Cardon M, et al. Fibroblast Heterogeneity and Immunosuppressive Environment in Human Breast Cancer. Cancer Cell. 2018;33:463–79.e10.
13. Dekkers JF, van Vliet EJ, Sachs N, Rosenbluth JM, Kopper O, Rebel HG, et al. Long-term culture, genetic manipulation and xenotransplantation of human normal and breast cancer organoids. Nat Protoc. 2021;16:1936–65.
14. Jia X, Liu H, Ren X, Li P, Song R, Li X, et al. Nucleolar protein NOC4L inhibits tumorigenesis and progression by attenuating SIRT1-mediated p53 deacetylation. Oncogene. 2022;41:4474–84.
15. Liu M, Ren Y, Zhou Z, Yang J, Shi X, Cai Y, et al. The crosstalk between macrophages and cancer cells potentiates pancreatic cancer cachexia. Cancer Cell. 2024;42:885–903.e4.
16. Hsu DS, Wang HJ, Tai SK, Chou CH, Hsieh CH, Chiu PH, et al. Acetylation of snail modulates the cytokinome of cancer cells to enhance the recruitment of macrophages. Cancer Cell. 2014;26:534–48.
17. Conn SJ, Pillman KA, Toubia J, Conn VM, Salmanidis M, Phillips CA, et al. The RNA binding protein quaking regulates formation of circRNAs. Cell. 2015;160:1125–34.
18. Piwecka M, Glazar P, Hernandez-Miranda LR, Memczak S, Wolf SA, Rybak-Wolf A. et al. Loss of a mammalian circular RNA locus causes miRNA deregulation and affects brain function. Science. 2017;357:eaam8526
19. Zheng Q, Bao C, Guo W, Li S, Chen J, Chen B, et al. Circular RNA profiling reveals an abundant circHIPK3 that regulates cell growth by sponging multiple miRNAs. Nat Commun. 2016;7:11215.
20. Abramson J, Adler J, Dunger J, Evans R, Green T, Pritzel A, et al. Accurate structure prediction of biomolecular interactions with AlphaFold 3. Nature. 2024;630:493–500.
21. Ma X, Lu C, Chen Y, Li S, Ma N, Tao X, et al. CCT2 is an aggrephagy receptor for clearance of solid protein aggregates. Cell. 2022;185:1325–45.e22.
22. Freund A, Zhong FL, Venteicher AS, Meng Z, Veenstra TD, Frydman J, et al. Proteostatic control of telomerase function through TRiC-mediated folding of TCAB1. Cell. 2014;159:1389–403.
23. Park SH, Jeong S, Kim BR, Jeong YA, Kim JL, Na YJ, et al. Activating CCT2 triggers Gli-1 activation during hypoxic condition in colorectal cancer. Oncogene. 2020;39:136–50.
24. Pohl C, Dikic I. Cellular quality control by the ubiquitin-proteasome system and autophagy. Science. 2019;366:818–22.
25. Hui CC, Angers S. Gli proteins in development and disease. Annu Rev Cell Dev Biol. 2011;27:513–37.
26. Kubo M, Nakamura M, Tasaki A, Yamanaka N, Nakashima H, Nomura M, et al. Hedgehog signaling pathway is a new therapeutic target for patients with breast cancer. Cancer Res. 2004;64:6071–4.
27. Neelakantan D, Zhou H, Oliphant MUJ, Zhang X, Simon LM, Henke DM, et al. EMT cells increase breast cancer metastasis via paracrine GLI activation in neighbouring tumour cells. Nat Commun. 2017;8:15773.
28. Lu L, Chen Z, Lin X, Tian L, Su Q, An P, et al. Inhibition of BRD4 suppresses the malignancy of breast cancer cells via regulation of Snail. Cell Death Differ. 2020;27:255–68.
29. Azenshtein E, Luboshits G, Shina S, Neumark E, Shahbazian D, Weil M, et al. The CC chemokine RANTES in breast carcinoma progression: regulation of expression and potential mechanisms of promalignant activity. Cancer Res. 2002;62:1093–102.
30. Qian BZ, Li J, Zhang H, Kitamura T, Zhang J, Campion LR, et al. CCL2 recruits inflammatory monocytes to facilitate breast-tumour metastasis. Nature. 2011;475:222–5.
31. Liu CX, Chen LL. Circular RNAs: Characterization, cellular roles, and applications. Cell. 2022;185:2016–34.
32. Zheng X, Huang M, Xing L, Yang R, Wang X, Jiang R. et al. The circRNA circSEPT9 mediated by E2F1 and EIF4A3 facilitates the carcinogenesis and development of triple-negative breast cancer. Mol Cancer. 2020;19:73
33. Shang Y, Huang EJ. Mechanisms of FUS mutations in familial amyotrophic lateral sclerosis. Brain Res. 2016;1647:65–78.
34. Errichelli L, Dini Modigliani S, Laneve P, Colantoni A, Legnini I, Capauto D, et al. FUS affects circular RNA expression in murine embryonic stem cell-derived motor neurons. Nat Commun. 2017;8:14741.
35. Wang R, Zhang S, Chen X, Li N, Li J, Jia R, et al. EIF4A3-induced circular RNA MMP9 (circMMP9) acts as a sponge of miR-124 and promotes glioblastoma multiforme cell tumorigenesis. Mol Cancer. 2018;17:166.
36. Guest ST, Kratche ZR, Bollig-Fischer A, Haddad R, Ethier SP. Two members of the TRiC chaperonin complex, CCT2 and TCP1 are essential for survival of breast cancer cells and are linked to driving oncogenes. Exp Cell Res. 2015;332:223–35.
37. Ghozlan H, Showalter A, Lee E, Zhu X, Khaled AR. Chaperonin-Containing TCP1 Complex (CCT) Promotes Breast Cancer Growth Through Correlations With Key Cell Cycle Regulators. Front Oncol. 2021;11:663877.
38. Zhang Z, Klionsky DJ. CCT2, a newly identified aggrephagy receptor in mammals, specifically mediates the autophagic clearance of solid protein aggregates. Autophagy. 2022;18:1483–5.
39. Pamudurti NR, Bartok O, Jens M, Ashwal-Fluss R, Stottmeister C, Ruhe L, et al. Translation of CircRNAs. Mol Cell. 2017;66:9–21.e7.
40. Li J, Ma M, Yang X, Zhang M, Luo J, Zhou H, et al. Circular HER2 RNA positive triple negative breast cancer is sensitive to Pertuzumab. Mol Cancer. 2020;19:142.
41. Iwai Y, Terawaki S, Honjo T. PD-1 blockade inhibits hematogenous spread of poorly immunogenic tumor cells by enhanced recruitment of effector T cells. Int Immunol. 2005;17:133–44.
42. Leach DR, Krummel MF, Allison JP. Enhancement of antitumor immunity by CTLA-4 blockade. Science. 1996;271:1734–6.
43. Hugo W, Zaretsky JM, Sun L, Song C, Moreno BH, Hu-Lieskovan S, et al. Genomic and Transcriptomic Features of Response to Anti-PD-1 Therapy in Metastatic Melanoma. Cell. 2016;165:35–44.
44. Spranger S. Tumor Heterogeneity and Tumor Immunity: A Chicken-and-Egg Problem. Trends Immunol. 2016;37:349–51.
45. Bonapace L, Coissieux MM, Wyckoff J, Mertz KD, Varga Z, Junt T, et al. Cessation of CCL2 inhibition accelerates breast cancer metastasis by promoting angiogenesis. Nature. 2014;515:130–3.
46. Ban Y, Mai J, Li X, Mitchell-Flack M, Zhang T, Zhang L, et al. Targeting Autocrine CCL5-CCR5 Axis Reprograms Immunosuppressive Myeloid Cells and Reinvigorates Antitumor Immunity. Cancer Res. 2017;77:2857–68.

47. Zhang Q, Qin J, Zhong L, Gong L, Zhang B, Zhang Y, et al. CCL5-Mediated Th2 Immune Polarization Promotes Metastasis in Luminal Breast Cancer. Cancer Res. 2015;75:4312–21.
48. Wu SZ, Al-Eryani G, Roden DL, Junankar S, Harvey K, Andersson A, et al. A single-cell and spatially resolved atlas of human breast cancers. Nat Genet. 2021;53:1334–47.
49. Sami E, Paul BT, Koziol JA, ElShamy WM. The Immunosuppressive Microenvironment in BRCA1-IRIS-Overexpressing TNBC Tumors Is Induced by Bidirectional Interaction with Tumor-Associated Macrophages. Cancer Res. 2020;80:1102–17.
50. Ueno T, Toi M, Saji H, Muta M, Bando H, Kuroi K, et al. Significance of macrophage chemoattractant protein-1 in macrophage recruitment, angiogenesis, and survival in human breast cancer. Clinical cancer research: an official journal of the American Association for. Cancer Res. 2000;6:3282–9.
51. Nalio Ramos R, Missolo-Koussou Y, Gerber-Ferder Y, Bromley CP, Bugatti M, Núñez NG, et al. Tissue-resident FOLR2(+) macrophages associate with CD8(+) T cell infiltration in human breast cancer. Cell. 2022;185:1189–207.e25.
52. Wagner J, Rapsomaniki MA, Chevrier S, Anzeneder T, Langwieder C, Dykgers A, et al. A Single-Cell Atlas of the Tumor and Immune Ecosystem of Human Breast. Cancer Cell. 2019;177:1330–45.e18.
53. Bassez A, Vos H, Van Dyck L, Floris G, Arijs I, Desmedt C, et al. A single-cell map of intratumoral changes during anti-PD1 treatment of patients with breast cancer. Nat Med. 2021;27:820–32.
54. Timperi E, Croizer H, Khantakova D, Rana M, Molgora M, Guerriero JL, et al. At the Interface of Tumor-Associated Macrophages and Fibroblasts: Immune-Suppressive Networks and Emerging Exploitable Targets. Clinical cancer research: an official journal of the American Association for. Cancer Res. 2024;30:5242–51.
55. Kieffer Y, Hocine HR, Gentric G, Pelon F, Bernard C, Bourachot B, et al. Single-Cell Analysis Reveals Fibroblast Clusters Linked to Immunotherapy Resistance in Cancer. Cancer Discov. 2020;10:1330–51.
56. Cords L, Tietscher S, Anzeneder T, Langwieder C, Rees M, de Souza N, et al. Cancer-associated fibroblast classification in single-cell and spatial proteomics data. Nat Commun. 2023;14:4294.
57. Pelon F, Bourachot B, Kieffer Y, Magagna I, Mermet-Meillon F, Bonnet I, et al. Cancer-associated fibroblast heterogeneity in axillary lymph nodes drives metastases in breast cancer through complementary mechanisms. Nat Commun. 2020;11:404.

ACKNOWLEDGEMENTS

This study was supported by grants from National Natural Science Foundation of China (82171854), the 2115 Talent Development Program of China Agricultural University, and Medical University of Bialystok, Poland (B.SUB.25.379).

AUTHOR CONTRIBUTIONS

Study concept and design: Xiangdong Li. Acquisition of data; analysis and interpretation of data: Lijun Zhou, Mei Liu, Fujun Liu, Zhengkun Wang, Xinyu Li, Xiaoyu Peng, Wenqiang Ma, Peilan Guo. Manuscript drafting: Lijun Zhou, Xiangdong Li. Critical revision of the manuscript for important intellectual content: Lifang Yuan, Slawomir Wolczynski, Nafis Ahmed Rahman, Wei Song, Xiangdong Li. Statistical analysis: Lijun Zhou.

COMPETING INTERESTS

The authors declare no competing interests.

ETHICS APPROVAL

All methods used to generate the data in this paper were performed in accordance with the relevant guidelines and regulations. The study protocols were approved by Ethics Committee of Shandong Provincial Hospital Affiliated to Shandong First Medical University (Approval number SWYX-NO. 2022-293), and informed consent was obtained from each donor. Animal Use and Care Committee of China Agricultural University approved the surgical interventions, treatments, and postoperative animal care procedures in this study (Approval number AW62201202-3-8, AW21214202-3-07, and AW71705202-3-01).

ADDITIONAL INFORMATION

Supplementary information The online version contains supplementary material available at https://doi.org/10.1038/s41388-025-03627-2.

Correspondence and requests for materials should be addressed to Xiangdong Li.

Reprints and permission information is available at http://www.nature.com/reprints

Publisher's note Springer Nature remains neutral with regard to jurisdictional claims in published maps and institutional affiliations.